Available online at www.sciencedirect.com
SCIENCE DIRECT®
Journal of Power Sources 119–121 (2003) 139–144
JOURNAL OF POWER SOURCES
www.elsevier.com/locate/jpowsour

Structural and electrochemical evaluation of $(1-x)Li_2TiO_3{\cdot}(x)LiMn_{0.5}Ni_{0.5}O_2$ electrodes for lithium batteries

Christopher S. Johnson*, Jeom-Soo Kim, A. Jeremy Kropf, Arthur J. Kahaian, John T. Vaughey, Michael M. Thackeray

Electrochemical Technology and Basic Sciences Program, Chemical Technology Division, Argonne National Laboratory, Argonne, IL 60439, USA

Abstract

X-ray diffraction (XRD), in situ X-ray absorption spectroscopy (XAS), and chemical lithiation experiments were used to evaluate the phases associated with the electrochemistry of the mixed-metal layered $LiMn_{0.5}Ni_{0.5}O_2$ oxide electrode. These results, along with coin-cell cycling data from the substituted layered $(1-x)Li_2TiO_3{\cdot}(x)LiMn_{0.5}Ni_{0.5}O_2$ composite oxide electrode are reported. The cycling behavior of $Li/0.05Li_2TiO_3{\cdot}0.95LiMn_{0.5}Ni_{0.5}O_2$ ($x = 0.95$) cells over an extended voltage window (4.3 or 4.6–1.25 V) under moderate current rate have yielded rechargeable capacities above 250 mAh/g. These large capacities and structural data suggest that both the composite $(1-x)Li_2TiO_3{\cdot}(x)LiMn_{0.5}Ni_{0.5}O_2$ and $LiMn_{0.5}Ni_{0.5}O_2$ (standard) layered electrodes operate predominantly off two-electron redox couples, Ni^{4+}/Ni^{2+} and Mn^{4+}/Mn^{2+}, approximately between 4.6 and 2.0 V, and between 2.0 and 1.0 V versus metallic Li, respectively. The $LiMn_{0.5}Ni_{0.5}O_2$ layered oxide is shown to reversibly react chemically or electrochemically with Li to form a stable, but air-sensitive dilithium compound, $Li_2Mn_{0.5}Ni_{0.5}O_2$ (Li_2MO_2; M = metal ion) that can be indexed to the space group $P\text{-}3m1$.

Keywords: Lithium batteries; Layered electrodes; Lithium–nickel–manganese oxides

1. Introduction

The synthesis, electrochemical, and structural properties of layered $(1-x)Li_2M'O_3{\cdot}(x)LiMO_2$ composite cathodes where M′ = Mn, Ti, Zr, Ru, and M = Mn, Ni, Co, are under investigation. This approach to stabilize layered $LiMO_2$ electrode structures emanated from earlier studies of the manganese system $(1-x)Li_2MnO_3{\cdot}(x)LiMnO_2$ that can be derived from the rock-salt phase Li_2MnO_3 by (1) acid-treatment to remove Li_2O and (2) relithiation of the $(1-x)Li_2MnO_3{\cdot}(x)MnO_2$ product by either chemical or electrochemical methods [1,2]. This research has demonstrated that a layered Li_2MnO_3 component (or an isostructural component, Li_2TiO_3 or Li_2ZrO_3) contributes to the stabilization of the layered $LiMnO_2$ electrode [3]. This approach has recently led to attempts to stabilize a layered $LiMn_{0.5}Ni_{0.5}O_2$ electrode [4,5] by incorporating a small amount of Li_2TiO_3 in a composite structure for $0 \leq x < 0.1$ [6]. Although $0.05Li_2TiO_3{\cdot}0.95LiMn_{0.5}Ni_{0.5}O_2$ electrodes did not improve the initial capacity loss effects that are observed when standard $Li/LiMn_{0.5}Ni_{0.5}O_2$ cells are cycled between 4.3 and 3 V (i.e. during break-in cycles), they displayed a higher coulombic efficiency on extended cycling between 4.6 and 2.5 V [6]. This has been attributed to a decrease in the oxygen activity at the surface of delithiated $0.05Li_2TiO_3{\cdot}0.95Li_{1-z}Mn_{0.5}Ni_{0.5}O_2$ ($0 < z \leq 1$) electrode particles at high states of charge.

In this paper, results of continued electrochemical and structural characterization of $(1-x)Li_2TiO_3{\cdot}(x)LiMn_{0.5}$-$O_2$ are reported for the composite electrode at $x = 0.95$. Of particular significance has been the observation that $Li/0.05Li_2TiO_3{\cdot}0.95LiMn_{0.5}Ni_{0.5}O_2$ and standard $Li/LiMn_{0.5}Ni_{0.5}O_2$ cells can be cycled over a large voltage window between 4.6 and 1.25 V with surprisingly good reversibility, leading to capacities in excess of 300 mAh/g [7,8]. To address the underlying factors associated with the large capacities observed, additional synthesis, XRD and XAS studies of the parent compound, $LiMn_{0.5}Ni_{0.5}O_2$, and the substituted composite $0.05Li_2TiO_3{\cdot}0.95LiMn_{0.5}Ni_{0.5}O_2$ electrode were conducted. Furthermore, we have obtained crystallographic data for the dilithium, layered compound, $Li_2Mn_{0.5}Ni_{0.5}O_2$, with hexagonal symmetry $P\text{-}3m1$ and report the results herein. The retention of a layered

* Corresponding author. Tel.: +1-630-252-4787; fax: +1-630-252-4176.
E-mail address: johnsoncs@cmt.anl.gov (C.S. Johnson).

0378-7753/03/$ – see front matter
doi:10.1016/S0378-7753(03)00143-5

$Mn_{0.5}Ni_{0.5}O_2$ framework and the lack of any significant formation of the Jahn–Teller ions, Mn^{3+} and Ni^{3+}, throughout the electrochemical or chemical reaction sequence are believed to be major contributing factors to the reversibility of this system between 4.6 and 1.25 V.

2. Experimental

The layered compound $0.05Li_2TiO_3{\cdot}0.95LiMn_{0.5}Ni_{0.5}O_2$ was prepared from a high-temperature reaction of lithium hydroxide, titanium dioxide (anatase), and a dihydroxide precursor $Mn_{0.5}Ni_{0.5}(OH)_2$ as described previously [6]. For comparison, the standard $LiMn_{0.5}Ni_{0.5}O_2$ was also prepared in an analogous manner. The as-prepared $LiMn_{0.5}Ni_{0.5}O_2$ material was also lithiated chemically with a 50 mol% excess of 0.1 M lithium naphthalide solution that had been freshly prepared from naphthalene and metallic lithium in tetrahydrofuran (THF) solvent at room temperature for 24 h. The product was filtered and washed in diethylether inside a nitrogen glovebox (<5 ppm H_2O), then subsequently transferred and stored in a recirculating/purifying He atmosphere (<5 ppm O_2) glovebox prior to X-ray diffraction analysis. The lithiated powder was loaded onto the sample holder and protected from moisture and air with a beryllium foil cover. The powder X-ray diffraction data of the $0.05Li_2TiO_3{\cdot}0.95LiMn_{0.5}Ni_{0.5}O_2$, $LiMn_{0.5}Ni_{0.5}O_2$ and lithiated product $Li_2Mn_{0.5}Ni_{0.5}O_2$ were collected on a Siemens D5000 powder diffractometer with Cu Kα radiation. Samples were scanned between 10 and 80° 2θ at a scan rate of 0.6° 2θ/min. Linear least-squares fit of the diffraction peaks was used to calculate unit cell parameters.

Electrodes were fabricated from an intimate mixture of the $0.05Li_2TiO_3{\cdot}0.95LiMn_{0.5}Ni_{0.5}O_2$ powder that comprised 85% by weight of the total electrode with 8% polyvinylidene difluoride polymer binder (Kynar) and 7% acetylene black in 1-methyl-2-pyrrolidinone. The electrode mixture was dried at 75 °C for 10 h, thoroughly ground and pressed into pellets on a stainless steel mesh (Exmet Corp.), and dried again under vacuum at 70 °C for 12 h. The electrodes were evaluated at room temperature in coin-type cells (size 2032, Hohsen) with a lithium foil counter electrode (FMC Corp., Lithium Div.), glass-fiber separator (Gelman Sciences) and an electrolyte consisting of a 1 M $LiPF_6$ solution in ethylene carbonate:diethylcarbonate (1:1) (Merck). Cells were constructed inside a He glovebox (<5 ppm, H_2O and O_2) and cycled on a Maccor Series 2000 tester under galvanostatic mode.

The cell current was interrupted every 30 or 40 min in order to determine cell impedance. Cyclic voltammetry (CV) data of a $LiMn_{0.5}Ni_{0.5}O_2$ electrode were collected to monitor the reversibility of the reaction between 2.5 and 1.0 V versus a metallic lithium reference electrode. These experiments were conducted with a PAR 273A potentiostat using CorrWare control software and a sweep rate of 0.05 mV/s.

A pouch-type cell was used for the in situ XAS experiments similar to that used in a previous $Li_xNi_{0.8}Co_{0.2}O_2$ cathode study [9]. Data were collected in transmission mode. The XAS measurements, which included both X-ray absorption near edge spectroscopy (XANES) and extended X-ray absorption fine structure (EXAFS) techniques, were performed on the insertion device (undulator A) beamline of the Materials Research Collaborative Access Team (MRCAT) at the advanced photon source (APS), Argonne National Laboratory. The details of the equipment and setup are reported in [9]. Nickel and manganese metal foils were used to calibrate the energy at each edge.

3. Results and discussion

The powder X-ray diffraction patterns of a standard $LiMn_{0.5}Ni_{0.5}O_2$ sample and a composite material $0.05Li_2TiO_3{\cdot}0.95LiMn_{0.5}Ni_{0.5}O_2$ are shown in Fig. 1. The XRD pattern of the parent layered compound $LiMn_{0.5}Ni_{0.5}O_2$ (Fig. 1a) with the Mn and Ni ions randomly distributed over the transition-metal sites is assigned to the α-$NaFeO_2$-structure type (rhombohedral space group *R*-3*m*); an ideal, random cation distribution would also make $LiMn_{0.5}Ni_{0.5}O_2$ isostructural with $LiNiO_2$ [10]. For $0.05Li_2TiO_3{\cdot}0.95LiMn_{0.5}Ni_{0.5}O_2$, a weak reflection at approximately 22° 2θ (Fig. 1b) indicates that a monoclinic (*C*2/*m*) Li_2TiO_3-type (or Li_2MnO_3-type) structure co-exists with the predominant $LiMn_{0.5}Ni_{0.5}O_2$ (*R*-3*m*) structure. It should be noted that in the structurally similar, layered oxide $Li_{1.2}Mn_{0.4}Cr_{0.4}O_2$ (or $0.4LiCrO_2{\cdot}0.4Li_2MnO_3$), localized clustering or domains of Li_2MnO_3 appear with layered $LiCrO_2$ (*R*-3*m*) [11]. Preliminary high-resolution transmission electron microscopy (HRTEM) data suggests that the addition of the Li_2TiO_3 rock-salt component to the structure subtly distorts the oxygen framework of the parent $LiMn_{0.5}Ni_{0.5}O_2$ structure to monoclinic symmetry [12].

In the standard layered $LiMn_{0.5}Ni_{0.5}O_2$ structure, the lithium atoms fill octahedral sites of one layer, while the nickel and manganese atoms fill the octahedral positions of adjacent layers. The XRD pattern of the chemically-lithiated $Li_2Mn_{0.5}Ni_{0.5}O_2$ phase, in which the strongest reflections

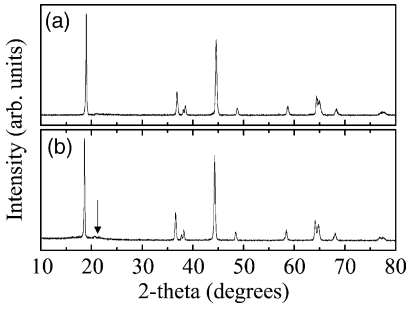

Fig. 1. XRD patterns of (a) as-prepared $LiMn_{0.5}Ni_{0.5}O_2$, and (b) $0.05Li_2TiO_3{\cdot}0.95LiMn_{0.5}Ni_{0.5}O_2$. Arrow marks the Li_2TiO_3 component contribution to the diffraction pattern.

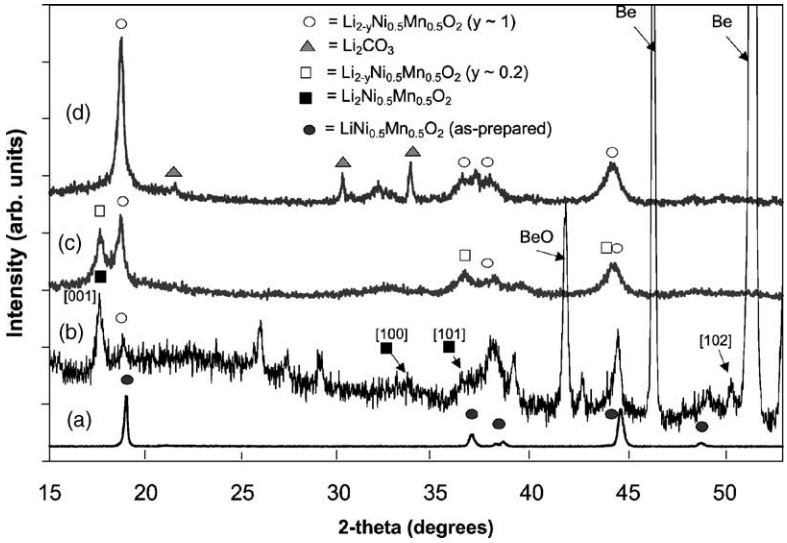

Fig. 2. XRD patterns of chemically lithiated $LiMn_{0.5}Ni_{0.5}O_2$, from bottom to top: (a) as-prepared starting material $LiMn_{0.5}Ni_{0.5}O_2$, (b) chemically lithiated $Li_2Mn_{0.5}Ni_{0.5}O_2$ under Be foil cover, (c) sample in b, after 2 h air exposure, and (d) sample in b after 10 h air exposure.

have been labeled, is shown in Fig. 2b; the pattern of the parent $LiMn_{0.5}Ni_{0.5}O_2$ is provided in Fig. 2a for comparison. In the $Li_2Mn_{0.5}Ni_{0.5}O_2$ structure, which has hexagonal symmetry P-3m1, the oxygen ions are arranged in a hexagonally-close-packed (hcp) array; the M ions are located in all the octahedral sites of one layer and the Li ions are located in all the tetrahedral sites of adjacent layers [13]. The [0 0 1] (or [0 1 0]) projection of the structure is shown in Fig. 3. In this structure, which has also been observed for Li_2NiO_2 [14] and Li_2MnO_2 [15], the Li^+–Li^+ distance in edge-shared tetrahedra is short (~2.2 Å) compared with the typical Li^+–Li^+ distances in edge-shared octahedra in related layered structures such as Li_2MnO_3 (2.70–2.92 Å) or $LiCoO_2$ (2.81 Å). Note that the peak in Fig. 2b at approximately 19° 2θ is associated with a small amount (less than 10%) of $LiMn_{0.5}Ni_{0.5}O_2$. The presence of some apparent unreacted material in the sample may be attributed either to an incomplete reaction, or to the instability of the highly lithiated structure and its tendency to extrude lithium at the particle surface when exposed to air, as discussed below.

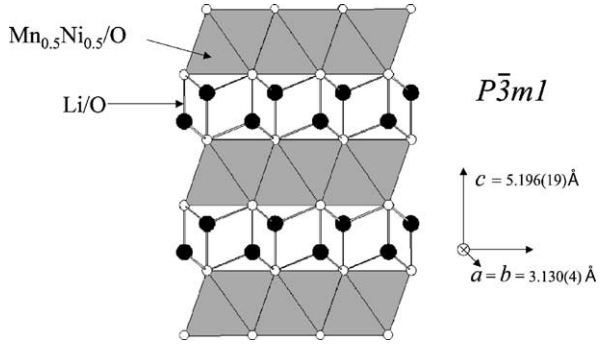

Fig. 3. The hexagonally-close-packed structure of $Li_2Mn_{0.5}Ni_{0.5}O_2$ showing the Mn^{2+} and Ni^{2+} ions in the octahedral sites of one layer and the Li^+ ions in the tetrahedral sites of adjacent layers.

The lattice parameters of $Li_2Mn_{0.5}Ni_{0.5}O_2$ are a = 3.130(4) Å, c = 5.196(19) Å; the corresponding volume of the unit cell, 44.09 Å^3 (Z = 1), represents an increase of ~22% in the crystallographic volume of the electrode for the two-phase reaction:

$$LiMn_{0.5}Ni_{0.5}O_2 + Li \rightarrow Li_2Mn_{0.5}Ni_{0.5}O_2$$

The $Li_2Mn_{0.5}Ni_{0.5}O_2$ product is air- and/or moisture-sensitive, and is easily oxidized. After 2 h exposure to air, it delithiates to form a two-phase product consisting of $Li_{2-y}Mn_{0.5}Ni_{0.5}O_2$ ($y \sim 1$) and a $Li_{2-y}Mn_{0.5}Ni_{0.5}O_2$ ($y \sim 0.2$) phase which is almost fully lithiated (Fig. 2c). From Rietveld analyses of the XRD patterns, it appears that a small range of solid-solution exists between the fully lithiated end-product $Li_2Mn_{0.5}Ni_{0.5}O_2$ and $Li_{2-y}Mn_{0.5}Ni_{0.5}O_2$ for $0 \leq y \leq 0.2$. The extruded lithium at the particle surface subsequently reacts with CO_2 in the air to form Li_2CO_3 leaving behind, after 10 h exposure to air, a reoxidized product with a stoichiometry close to the parent $LiMn_{0.5}Ni_{0.5}O_2$ material, as shown in Fig. 2d.

It is interesting to note that the lithiation and delithiation reactions described above do not produce any Mn(III)-associated secondary phases, such as the commonly observed Li–Mn–O spinel-type phases. Furthermore, no obvious Ni and/or Mn displacement reactions occur during the chemical reaction of $LiMn_{0.5}Ni_{0.5}O_2$ with lithium naphthalide. The retention and robustness of the layered $Mn_{0.5}Ni_{0.5}O_2$ framework is a unique feature of the reaction, even though the material after re-oxidation becomes less crystalline. A detailed description of the charge compensation mechanism involved at low voltages for the Li($Mn_{0.5}$-$Ni_{0.5}$)O_2-to-Li_2($Mn_{0.5}Ni_{0.5}$)O_2 transition has been reported previously in an XAS in situ cell study [8].

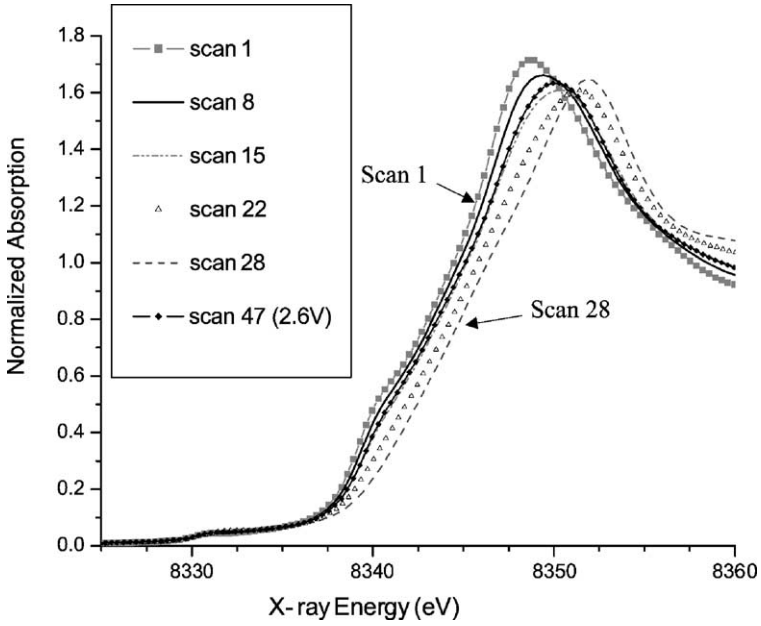

Fig. 4. Calibrated and normalized XANES data (Ni K edge). Reproducibility of the calibration is ±0.05 eV. Scan number refers to the X-ray absorption scan taking place over the Ni and Mn K edge energies. The scan is approximately 9.2 min in length to complete. Electrochemical data is as follows: scan 1 is taken at OCV and was 3.6 V for the cell at the beginning of charge; scan 8 (3.81 V, 58 mAh/g), scan 15 (4.02 V, 107 mAh/g), scan 22 (4.33 V, 157 mAh/g). Scan 28 is the final charge cutoff voltage of 4.6 V (200 mAh/g). Scan 47 is associated with the voltage at 2.6 V at the end of the subsequent discharge (147 mAh/g).

In situ XANES data of a standard $Li_{1-x'}Mn_{0.5}Ni_{0.5}O_2$ electrode in a lithium pouch cell were first collected in the higher voltage window (4.6–2.5 V). The Ni K edge spectra for this experiment are shown in Fig. 4. A gradual Ni K edge shift to higher energy totaling approximately 2 eV was observed for the electrode during the initial charge at room temperature from 3.6 to 4.6 V (4.3 h charge, current = 46.5 mA/g). In contrast, there was essentially no shift observed for the Mn metal center (data not shown). The charge capacity was 200 mAh/g, which corresponds to $x' = 0.71$ and an average Ni oxidation state of 3.4+. The Mn K edge traces that of the Li_2MnO_3 standard (Mn^{4+}) throughout this whole voltage window. Qualitative K edge comparisons against NiO, $LiNiO_2$, and $LiNi_{0.8}Co_{0.2}O_2$ standards suggest that a nominal average oxidation state change from about 2.3–3.2 occurs exclusively at the Ni metal center site. The process is reversible because the Ni K edge returns almost to its original position when the cell is discharged to 2.6 V (Fig. 4, scan 47; 3.1 h discharge, current = 46.5 mA/g; 147 mAh/g). In the data collected at lower voltages, the Ni K edge is observed to continue to shift back to lower energy during further discharge, finally stopping at about 1.4 V [8]. At this voltage, the Ni K edge position nearly matches that of the NiO (divalent Ni^{2+}) standard.

It should be noted that XANES presents only an average composition for the sample. Thus, during electrochemical cycling in the upper voltage range, the Ni oxidation state could be defined either as a 40/60% percentage ratio of 2+/4+ at the top of charge, or, in another interpretation, simply delocalized as 3.2+ in 100% of the sample. First principles calculations, however, suggests that the charge distribution for $LiNi_{0.5}Mn_{0.5}O_2$ is best represented as a mixed-valent compound consisting of Ni^{2+} and Mn^{4+} [16]. Curve fitting and analysis of the EXAFS data (nearest neighbor bond lengths, transition-metal coordination numbers and symmetry) is in progress to definitively determine the charge compensation process and its details during cycling [17].

To evaluate the electrochemical reversibility of $0.05Li_2TiO_3{\cdot}0.95LiMn_{0.5}Ni_{0.5}O_2$ composite electrodes at moderate rates (25 mA/g), cycling experiments were conducted over an extended voltage window. Fig. 5a shows the results of cycling a $Li/0.05Li_2TiO_3{\cdot}0.95LiMn_{0.5}Ni_{0.5}O_2$ cell, after an initial charge to 4.3 V, between 4.6 and 1.25 V for four cycles. The cycling was conducted at 50 °C to aid the electrode kinetics for the two-phase reaction at low voltages [8]. After delivering 163 mAh/g on the initial charge, the electrode yielded a capacity of 284 mAh/g on the subsequent discharge. The cell faded to 246 mAh/g discharge capacity on the 5th discharge, representing a fade rate of 2.7% loss per cycle. Thereafter, the charge cut-off voltage was increased from 4.3 to 4.6 V (Fig. 5b), and the cell cycled for another 5 cycles. The specific capacity increased on discharge to 278 mAh/g and then faded to 260 on the 10th cycle, representing a fade rate of 1.3% loss per cycle. Coulombic efficiencies throughout these cycling tests remained steady at an excellent 99%. A greater capacity can be achieved if the lower voltage cut-off is set below 1.25 V. However, when lower cut-off voltages are used, e.g. 1.0 V, we have noted that the reversibility of the system is

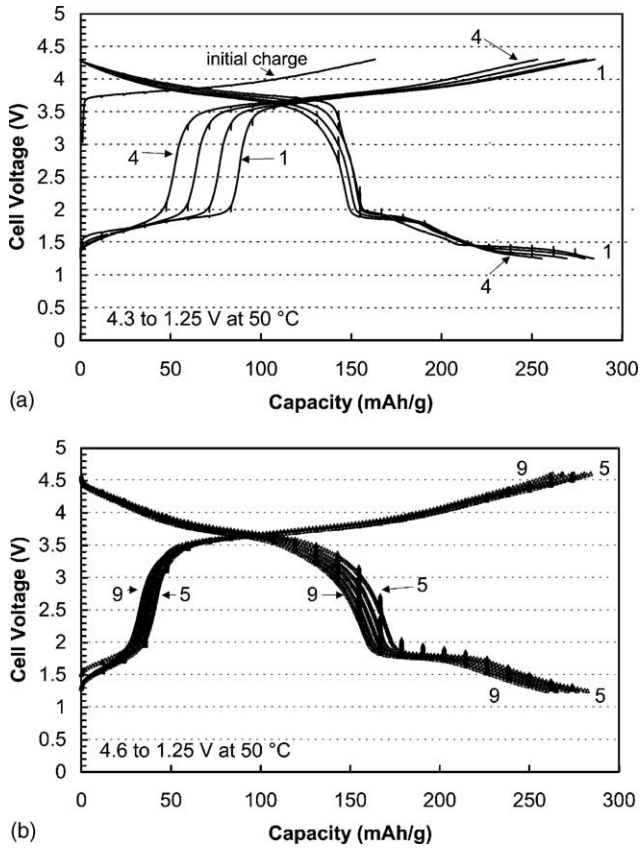

Fig. 5. Voltage profiles of a Li/0.05Li_2TiO_3·0.95$LiMn_{0.5}Ni_{0.5}O_2$ cell between (a) 4.3 and 1.25 V, and (b) 4.6 and 1.25 V at 50 °C.

compromised by the greater possibility of displacing Ni and/or Mn from the oxide structure.

A cyclic voltammogram (Fig. 6) of a 0.05Li_2TiO_3·0.95-$LiMn_{0.5}Ni_{0.5}O_2$ electrode limited to the voltage range 2.5–1.0 V shows that the reaction to form the highly lithiated Li_2MO_2 phase at the electrode surface is reversible, but that considerable peak broadening occurs, particularly during reduction, after the initial sweep.

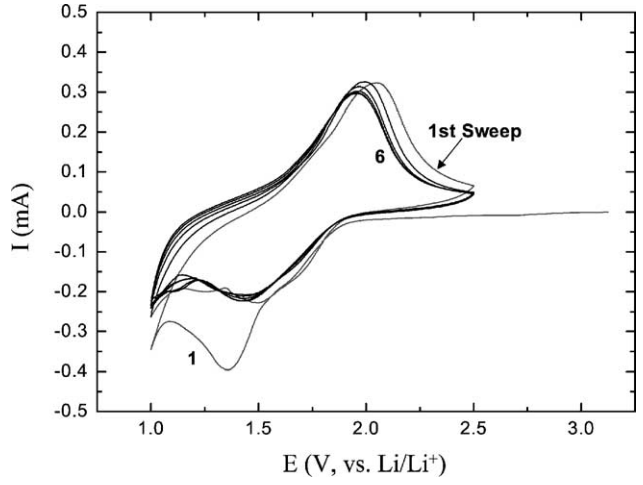

Fig. 6. Cyclic voltammograms at room temperature of a 0.05Li_2TiO_3·0.95$LiMn_{0.5}Ni_{0.5}O_2$ electrode between 2.5 and 1.0 V (scan rate = 0.05 mV/s).

4. Conclusions

Synthesis and characterization of the lithiated product of $LiMn_{0.5}Ni_{0.5}O_2$ was conducted. The XRD and XAS results, together with electrochemical cycling data, suggest that $LiMn_{0.5}Ni_{0.5}O_2$ layered electrodes operate predominantly off two-electron redox couples, Ni^{4+}/Ni^{2+} and Mn^{4+}/Mn^{2+}, between 4.5 and 2.0 V and between 2.0 and 1.25 V versus metallic Li, respectively. The apparent absence of any significant amount of the Jahn–Teller ions, Ni^{3+} and Mn^{3+} in the high- or low-voltage region may be a factor that contributes to the excellent structural and electrochemical stability of these electrodes. The $LiMn_{0.5}Ni_{0.5}O_2$ is shown by XRD to form a stable, but air-sensitive dilithium compound, $Li_2Mn_{0.5}Ni_{0.5}O_2$ with hexagonal symmetry, *P*-3*m*1. The reaction is reversible, both chemically and electrochemically. The cycling behavior of composite Li/0.05Li_2TiO_3·0.95$LiMn_{0.5}Ni_{0.5}O_2$ cells over an extended voltage window (4.3 or 4.6–1.25 V) was studied. These results demonstrate that rechargeable capacities above 250 mAh/g can be obtained at a 25 mA/g current rate. By understanding the electrochemical properties and structures of Ni–Mn mixed-metal layered oxides, we can begin to integrate the lithiated-layered structure Li_2MO_2 (M = metal ion) into new battery design concepts and technologies. Thus, these new findings have broad implications for improving the electrochemical performance of lithium-ion cells because it may be possible to eliminate the first cycle capacity loss in graphite, alloy or intermetallic Li-ion full cells by exploiting the Li_2MO_2 phase in a sacrificial first charge.

Acknowledgements

Support from the Office of Basic Energy Sciences, Division of Chemical Sciences, and the Office of Advanced Automotive Technologies, both of the US Department of Energy, under Contract No. W31-109-ENG-38, is gratefully acknowledged. Use of the Advanced Photon Source was supported by the US Department of Energy, Basic Energy Sciences, and the Office of Science (DOE-BES-SC), under Contract No. W-31-109-ENG-38. Work performed at MRCAT is supported, in part by funding from the Department of Energy under grant number DEFG0200ER45811.

References

[1] M.H. Rossouw, D.C. Liles, M.M. Thackeray, J. Solid State Chem. 104 (1993) 464.
[2] C.S. Johnson, M.M. Thackeray, Electrochem. Soc. Inc. Proc. PV 2000-36 (2001) 47.

[3] C.S. Johnson, S.D. Korte, J.T. Vaughey, M.M. Thackeray, T.E. Bofinger, Y. Shao-Horn, S.A. Hackney, J. Power Sources 81–82 (1999) 491.
[4] T. Ohzuku, Y. Makimura, Chem. Lett. (2001) 744.
[5] Z. Lu, D.D. MacNeil, J.R. Dahn, Electrochem. Solid-State Lett. 4 (2001) A191.
[6] J.-S. Kim, C.S. Johnson, M.M. Thackeray, Electrochem. Commun. 4 (2002) 205.
[7] C.S. Johnson, J.-S. Kim, A.J. Kropf, J.T. Vaughey, M.M. Thackeray, 11IMLB Book of Abstracts, Abstract No. 119, The Electrochemical Society, 23–29 June 2002.
[8] C.S. Johnson, A.J. Kahaian, J.-S. Kim, A.J. Kropf, J.T. Vaughey, M.M. Thackeray, Electrochem. Commun. 4 (2002) 492.
[9] C.S. Johnson, A.J. Kropf, Electrochim. Acta 47 (2002) 3187.
[10] M. Marezio, J.P. Remeika, J. Chem. Phys. 44 (1966) 3348.
[11] B. Ammundsen, J. Paulsen, I. Davidson, R.-S. Liu, C.-H. Shen, J.-M. Chen, L.-Y. Jang, J.-F. Lee, J. Electrochem. Soc. 149 (2002) A431.
[12] S.A. Hackney, J.-S. Kim, C.S. Johnson, M.M. Thackeray, 2002, unpublished data.
[13] H. Rieck, R. Hoppe, Z. Anorg. Allg. Chem. 392 (1972) 193.
[14] J.R. Dahn, U. von Sacken, C.A. Michal, Solid State Ionics 44 (1990) 87.
[15] W.I.F. David, J.B. Goodenough, M.M. Thackeray, M.G.S.R. Thomas, Rev. Chem. Miner. 20 (1983) 636.
[16] J. Reed, G. Ceder, Electrochem. Solid-State Lett. 5 (2002) A145.
[17] C.S. Johnson, A.J. Kropf, J.-S. Kim, M.M. Thackeray, 2002, unpublished data.